

Apoptotic Cell Death in Cultured Cardiomyocytes Following Exposure to Low Concentrations of 4-Hydroxy-2-nonenal

María P. Hortigón-Vinagre · Fernando Henao

Published online: 11 March 2014
© Springer Science+Business Media New York 2014

Abstract Lipid peroxidation (LP), induced by oxidative stress, is associated with degenerative processes. 4-Hydroxy-2-nonenal (HNE), a highly reactive diffusible product of LP, is considered by-product and mediator of oxidative stress. Its level increases under pathological conditions such as cardiovascular diseases. In this study, we partially characterized the mechanisms of HNE-mediated cytotoxicity in cardiomyocytes. After establishing that pathophysiological doses of HNE trigger cell death dependent on the incubation time and dose of HNE ($LD_{50} = 4.4 \mu\text{M}$), we tackled the mechanisms that underlie the cell death induced by HNE. Our results indicate that HNE rapidly increases intracellular Ca^{2+} ; it also increases the rate of reactive oxygen species generation and causes a loss of mitochondrial membrane potential ($\Delta\Psi\text{m}$) as well as a decrease in the ATP and GSH levels. Such alterations result in the activation of caspase-3 and DNA breakdown, both characteristic features of apoptotic cell death, as well as disruption of the cytoskeleton. Moreover, the nucleophilic compounds *N*-acetyl-cysteine and β -mercapto-propionyl-glycine, and the synthetic antioxidant Trolox exert a potent antioxidant action against HNE damage; this suggests its use as effective compounds in order to reduce the damage occurred as consequence of cardiovascular disorders in which oxidative stress and hence LP take place.

Keywords Cardiomyocytes · 4-Hydroxy-2-nonenal · Calcium · ROS · Mitochondria · Apoptosis

Introduction

Oxidative stress mechanisms have a central role in the pathogenesis of cardiovascular and chronic diseases and also play a major role in the aging process [1]. In the context of membrane biology, reactive oxygen species (ROS) production damages lipidic cell membranes by the process of lipid peroxidation (LP), in which several aldehydes, including 4-hydroxy-2-nonenal (HNE), are generated, HNE being the most reliable marker of LP [2, 3]. The heart is a highly oxidative organ due to its high mitochondria content; therefore, it is particularly vulnerable to the accumulation of LP products, such as HNE, which are formed as a result of oxidative damage [4].

HNE can markedly induce a positive feedback loop of intracellular production of ROS [3], as well as alter Ca^{2+} dynamics; a fact described by our group in sarcoplasmic reticulum (SR) vesicles [5]. In recent years, research identified HNE as a particularly important mediator and marker of cellular dysfunction and degeneration in a wide range of disorders including cardiovascular diseases [6].

HNE has a number of implications on CVDs. High levels of HNE have been described in atherosclerotic lesions of human subjects and in animal models of cardiovascular disease, where HNE promotes macrophage foam cell formation [7]. HNE is implicated in myocardial infarction (MI), which could be considered a direct consequence of atherosclerotic lesions in the coronary arteries. MI, besides being a harmful disease, may finally result in heart failure (HF) and subsequent death [8]. Persistent

Electronic supplementary material The online version of this article (doi:10.1007/s12012-014-9251-5) contains supplementary material, which is available to authorized users.

M. P. Hortigón-Vinagre · F. Henao (✉)
Departamento de Bioquímica y Biología Molecular y Genética,
Facultad de Ciencias, Universidad de Extremadura,
06071 Badajoz, Spain
e-mail: fhenao@unex.es

ischemia in MI results in necrotic cell death—the restoration of blood flow being the most effective method of limiting necrosis. However, the effects of reperfusion itself may also be associated with tissue injury [9]. Reperfusion is associated with a burst of ROS production as well as a calcium overload. The mechanisms that underlie cell death after reperfusion are not well established, despite the fact that a large collection of experimental data supports the presence of apoptosis as the most important mechanism of cell death during reperfusion [10].

Cell death plays a key role in a variety of cardiovascular diseases due to loss of terminally differentiated cardiac myocytes, in which have been described mechanisms of apoptosis and necrosis [11]. Apoptosis has been considered an active and regulated form of cell death, characterized by a number of distinct morphological and molecular changes [12]. In contrast, necrosis has been considered to be an accidental, uncontrolled, and passive form of cell death [12].

The fact that HNE induces apoptosis in other cell types has been demonstrated [13]. The decrease in intracellular HNE levels prevents the apoptotic process [14]. In cells, conjugation of HNE with GSH is the major detoxification mechanism for HNE [2]. The depletion of GSH renders cells more vulnerable to cell death [15]. In many cases, it is well established that cell death caused by oxidative stress and LP is preceded by depletion of intracellular GSH [16].

The experiments presented in this paper are based on three inter-related observations: (a) the exposure of cardiomyocytes to oxidative stress underlies the beginning and development of CVDs [17], (b) there is correlation between CVD and HNE, since high HNE concentrations are described in heart under ischemia/reperfusion (I/R) and/or HF [8], and (c) HNE, among other causes, produces a deregulation of the homeostasis of intracellular calcium which can lead to cell death [18]. The evidence obtained indicates that HNE could mediate important deleterious effects on cardiac myocytes, playing a key role in the cell death associated with CVDs, especially in I/R and subsequent HF. Moreover, it will be very useful to find cardioprotective agents, such as antioxidant compounds, directed against HNE, as a therapeutic strategy to reduce the myocardial damage induced by CVDs.

Materials and Methods

Preparations of HNE Solutions

A stock solution of HNE was always prepared by dilution of a commercial HNE solution (Ref: 393204 CALBIO-CHEM) in dimethyl sulfoxide (DMSO). The DMSO added to the culture was lower than 0.1 % v/v, in every case.

Culture of Neonatal Rat Cardiomyocytes

Primary cultures of cardiac myocytes were prepared by the method previously described in [19]. Briefly, ventricles from hearts of neonatal (1–3 days old) Wistar rats (*Rattus norvegicus*) killed by decapitation (10–14 pup rats born from adult rats who were provided of food and water ad libitum, and the lighting conditions were controlled—12 h light and 12 h dark) were dissociated with pancreatin and collagenase. The cells were resuspended in Dulbecco's modified Eagle's medium (DMEM) and medium 199 (ratio 4:1) supplemented with 10 % horse serum, 5 % fetal bovine serum, 2 mM L-glutamine, 100 U/mL penicillin, and 100 U/mL streptomycin (growth medium). To selectively enrich the myocytes, dissociated cells were preplated for 2 h in large plastic dishes (10-cm-diameter, Corning) (37 °C, 5 % CO₂, water-saturated air atmosphere) to remove most of the rapidly adhering non-muscle cells. Following preplating, the resultant suspension of myocytes was transferred onto fibronectin- and collagen-coated (0.002 mg/mL fibronectin and 0.018 mg/mL collagen) culture dishes, at a density of 1×10^6 cells/35-mm dish. The mitotic inhibitor cytosine- β -D-arabino-furanoside (AraC), in a final concentration of 20 μ M, was added during the first 24 h to block non-myocytes cell proliferation. After 3 days in growth medium at 37 °C, the cardiomyocytes were switched to serum-free medium. All experiments were performed using cardiomyocytes at 3–4° DIV (days in vitro). For microscopy experiments, the cells were seeded onto fibronectin- and collagen-coated sterilized glass coverslips. In this case, the density of the culture was increased to 1.5×10^6 cells/35-mm dish, due to the difficulty of attaching. The purity of culture was determined by cell counting. Cardiomyocytes were distinguished from non-muscle cells in base of anti- α -actinin positive stained for the cardiomyocytes. Another criterion that led us to differentiate both cell types was the nucleus size, which in non-muscle cells is larger than in cardiomyocytes. A level of purity higher than 90 % was established in our culture (Supplementary Material, Figure S1). The experiments involving animals have been carried out in accordance with the EU Directive 2010/63/EU for animal experiments and approved in compliance with the guidelines established by the Animal Care and Use Committee of the University of Extremadura.

Immunofluorescence and Rhodamine–Phalloidin Staining

For immunofluorescence, cells were fixed for 15 min at room temperature in 4 % paraformaldehyde (Polysciences, Warrington, PA) and permeabilized for 4 min with 0.1 % Triton X-100. After blocking the unspecific epitopes with

0.1 % PBS:BSA for 30 min, cells were immunostained with the antibodies for α -tubulin (Sigma, Ref 18-0092) or anti- α -actinin sarcomeric (Sigma, Ref A7732) both at 1:200 during 1 h. The secondary fluorescence antibody was anti-mouse-Alexa 488 (Invitrogen, dilution 1:200, 1 h in darkness). To label actin fibers, NRC were also stained with 0.25 units of rhodamine-phalloidin (Invitrogen) per coverslip for 30 min (darkness). Nuclei were stained with 2 μ M DAPI (5 min). Images were taken using an Olympus fluorescence microscope with magnifications of 20 \times and 40 \times .

Cell Viability Determination by MTT Reduction and Trypan Blue Exclusion Assay

Changes in cell viability were determined using the 3-[4,5-dimethylthiazol-2-yl]-2,5-diphenyl-tetrazolium (MTT) reduction assay as described in [20]. In brief, NRC grown on 24-well plates (2.5×10^5 cells/well) for 4 days were depleted of serum during 12 h, treated with HNE or not, and incubated with 500 μ L of 0.15 mg/mL MTT solution per well in Locke K5 (154 mM NaCl, 4 mM NaHCO₃, 5 mM KCl, 10 mM HEPES pH 7.4/NaOH, 5 mM glucose, 2.3 mM CaCl₂, 1 mM MgCl₂) for 30 min in a CO₂ incubator. After removing MTT solution, 250 μ L of DMSO was added to dissolve the blue formazan crystals produced by the reduction of MTT. The formazan generated was quantified by measuring the difference in absorbance between 490 and 700 nm using a spectrophotometer UV mini 1240 (Shimadzu). Additionally, changes in cell viability were determined by the trypan blue exclusion assay as previously described in [21]. Cells in 4^o DIV were depleted of serum during 12 h, incubated with trypan blue dye at 0.4 % (w/v) for 4 min, and then washed with PBS to eliminate excess of dye. Cells not stained were considered as viable cells. Blue-stained cells with swollen soma were classified as dead cells. To quantify cell death, a minimum of 500 cells were counted in 4–5 microscopic fields per plate. Three separate cultures and a minimum of two plates per condition were used.

Quantification of Reduced Glutathione Content

The measurement of reduced glutathione content of neonatal rat cardiomyocytes was taken as described in [20]. Briefly, after removal of cell culture medium, NRC were lysed in ice-cold 10 mM Tris, 1 mM EDTA supplemented with 10 % perchloric acid, and precipitated proteins were removed by 10-min centrifugation at 12,000 \times g at 4 $^{\circ}$ C. Thereafter, total and oxidized glutathione measurements in the supernatant were taken as indicated in [20], using 5,5'-dithiobis(2-nitrobenzoic acid) and the recycling system (glutathione reductase + NADP(H)).

Measurements of ADP/ATP Ratio

Adenine nucleotides were determined spectrophotometrically as described in [20] after extraction with perchloric acid and neutralization with KOH [20].

Measurements of LDH Release

Cardiac myocyte plasma membrane integrity was assessed by measuring the release of LDH into the culture medium, as is indicated in [22]. Briefly, after removing the medium, which was used as reference in the following step, the cells were lysed by the addition of 1 % Triton X-100. The lysed cells and the medium were centrifuged at 1,500 \times g for 3 min, and supernatants were used to determine the LDH activity. Samples were added to a cuvette containing 50 mM Tris-HCl pH 7.4, 1 mM sodium pyruvate, and 0.15 mM NAD(H). The oxidation of NAD(H) by LDH activity was determined spectrophotometrically at 340 nm. Results were expressed as ratio LDH_{free}/LDH_{total}. The LDH_{total} is LDH_{free} + LDH_{cyt}.

Measurements of active caspase-3

Cultures (seeded on glass coverslips coated with fibronectin and collagen) were washed in PBS and incubated at 37 $^{\circ}$ C for 30 min with 1 μ L/mL of the caspase-3-specific substrate (FITC-DEVD-FMK, CaspGLOW Fluorescein Active Caspase-3 Staining kit, BioVision). After an additional wash with “wash buffer,” cells were analyzed using an Olympus FV1000 confocal microscope using 488-nm laser line for excitation and BP530/30 for emission detection. NRC treated with 10 μ M HNE in the presence of caspase inhibitor Z-VAD (1 μ L/mL, as is indicated in the kit) were used as a negative control for caspase-3 activity and to demonstrate the specificity of the method. Positive cells were counted in 20 different fields (20 \times). Data are represented as positive cell versus total cell number in percentage.

Assessment of Apoptosis by DNA Cell Cycle Analysis by Flow Cytometry Using Vindelov's Reagent

Cell cycle distribution in NRC was determined after staining the DNA with propidium iodide (PI). Nuclei were obtained with Vindelov's solution (10 mM Tris pH 8, 10 mM NaCl, 0.1 mg/mL RNase, and 0.1 % Tween-20). After staining nuclei with 0.003 % w/v PI, samples were transferred to the FC-500 flow cytometer (Beckman Coulter), and cell fluorescence was measured. In each experiment, at least 10,000 cells were counted. The area versus the width of the fluorescence signal was analyzed to gate out cellular multiples. Histograms of DNA content

were analyzed with SUMMIT 5.0 software (Beckman Coulter, Hialeah, FL) to determine fractions of the population in each phase of the cell cycle (G_0 , G_1 , S, and G_2/M). The analysis of the sub- G_0 fraction to determine hypodiploidy was used as a marker of DNA breakdown as a consequence of apoptosis onset. For cell cycle analysis, only signals from single cells were considered.

Determination of Mitochondrial Membrane Potential ($\Delta\Psi_m$) by Live Imaging

The cells grown in 15-mm glass coverslips were treated with HNE or DMSO for 1 h at 37 °C in medium Locke K5, washed with PBS 1×, and loaded with 2 nM TMRM and 10 µg/mL Hoechst 33342 for 30 min at 37 °C. Intracellular TMRM fluorescence was visualized and recorded using an FV 1000 Olympus laser scanning confocal microscopy. To quantify, TMRM positive cell number versus total cell number was used. Excitation and emission wavelengths were 550/590 nm for TMRM for mitochondrial membrane potential detection and 405/440 nm for nuclei stained with Hoechst 33342. Images were acquired using a 40× objective.

Assay of ROS Formation

The cells grown in 15-mm glass coverslips were treated with HNE or DMSO for 1 h at 37 °C in medium Locke K5 and washed with PBS 1×. The load with 0.4 µM DCFH-DA and 10 µg/mL Hoechst 33342 (to stain nuclei from viable cells) in PBS 1× was performed during the treatment; 3.75 µM PI was added just 5 min before finishing the time of loading with the dyes to stain nuclei from death cells. Afterward, coverslips were visualized and recorded using an FV 1000 Olympus laser scanning confocal microscopy. To quantify, DCF positive cell number versus total cell number was used. Excitation and emission wavelengths were 488/525 nm for DCF, 405/440 nm for Hoechst 33342, and 488/650 nm for PI. Images were acquired using a 40× objective.

Measurement of the Cytosolic Ca^{2+} Concentration

Intracellular Ca^{2+} concentration ($[Ca^{2+}]_i$) was measured as is indicated in [20]. The cells were loaded with 5 µM fura-2-AM in serum-free medium at 37 °C for 45 min. Afterward, cells were washed twice with Locke K5 and treated in the same medium with HNE or DMSO. To measure $[Ca^{2+}]_i$, ratiometric fluorescence images were obtained with excitation filters of 340 and 380 nm. The emission was recorded at 510 nm with an epifluorescence microscope (Cell R, Olympus).

Statistical Analysis

The data are given as the mean \pm SD. Statistical analysis was carried out using one-way analysis of variance (ANOVA) followed by Tukey's test. Significant differences were considered when $p \leq 0.05$.

Results

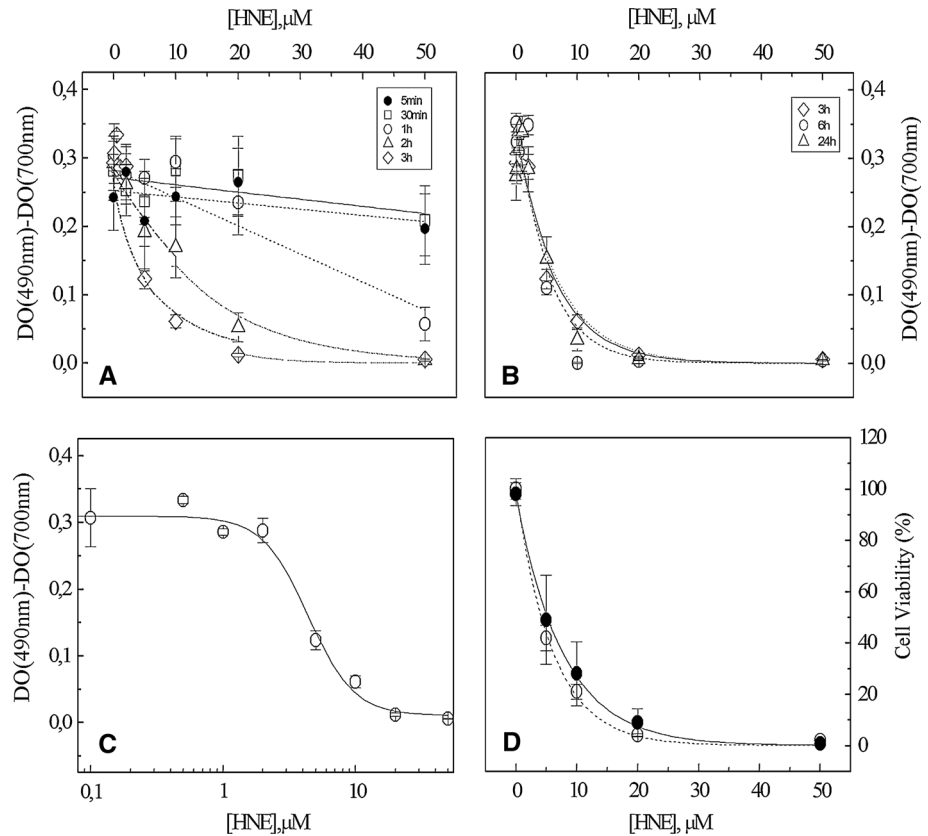
Effects of HNE on Cell Viability and Protection by NAC, MPG, and Trolox

The MTT assay revealed that treatment of cardiac myocytes with HNE resulted in a significant reduction in viable cells compared with control (incubation with DMSO, HNE vehicle). Figure 1 shows that loss of cell viability is dose and time dependent (Panel A), peaking at 3 h (Panel B). After 3-h treatment with 10 µM HNE, only 10 % of cultured cells remain alive. At this incubation time, the LD_{50} has been established to be 4.4 µM (Fig. 1c). The results obtained by the MTT assay were supported by trypan blue exclusion method, as illustrated in Fig. 1d, in which no significant differences are found between both methodologies. This set of experiments showed the vulnerability of neonatal rat cardiomyocytes to small doses of HNE (<10 µM), which are included in the range of HNE concentration detected in the plasma serum of CVD patients, such as MI or HF, which has been demonstrated to be 22.2 ± 3.36 µM (together with MDA) and 0.5 µM, respectively [23, 24].

In order to investigate whether thiol compounds, NAC or MPG, which have the ability to terminate free radical chain reactions and/or to directly sequester free HNE, could protect against HNE-induced NRC cell death, the cardiomyocytes were preincubated for 3 h with 1 mM NAC or MPG before treatment with 5 or 10 µM HNE in Locke medium (serum-free medium contained thiol compounds is replaced by fresh Locke medium supplemented with HNE or DMSO to assure the absence of NAC or MPG in the extracellular medium). The decrease in viable cells induced by HNE treatment was significantly suppressed by pretreatment of NRC with NAC or MPG 1 mM, leading to a cell viability which in the case of 5 µM HNE was not different from untreated controls, whereas the extent of protection is lower, although significant, when the cells were treated with 10 µM HNE (Fig. 2a).

In addition, we also tested the antioxidant Trolox, showing in this case a higher protective effect compared with NAC or MPG. When cardiac myocytes are pre- or co-incubated with Trolox 0.2 mM, both conditions almost completely prevent the cell death induced by 5 and 10 µM

Fig. 1 HNE induces cell death in cultured NRC: After 4° DIV, cells plated at 1×10^6 cells into 35-mm-diameter dishes were transferred to a serum-free medium, and 12 h later, they were treated with different HNE concentrations in Locke K5 medium. The incubation times are indicated in **a** and **b**. In **c** and **d**, the incubation time was 3 h. The viability was assessed by MTT reduction in all cases except for the *full circles* of **d**, where the trypan blue exclusion method was employed



HNE, but co-incubation was the most effective condition, as shown in Fig. 2b.

HNE Depletes Intracellular GSH

It is well known that GSH acts as the first defensive line against HNE damage, due to its cysteine thiol group, which acts as a nucleophile in reactions with electrophilic species, such as HNE [2]. Maintaining the GSH pool is critical for cell survival, an imbalance of GSH being a common feature in a wide range of pathologies [25]. Therefore, as expected (and taking into account our previous work [5], in which HNE causes the depletion of thiol residues in SERCA1a), the GSH content was significantly depleted in cardiomyocytes exposed to HNE. The GSH content in NRC decreases by 80 % after treatment with 5 μM HNE for 3 h, as it is shown in Fig. 3a (filled circles). The pre-treatment with 1 mM NAC or MPG (open symbols Fig. 3a) completely prevents loss of the GSH pool, NAC being marginally more efficient. This could be explained by the fact that NAC can act as a precursor of GSH [26]. Besides the content of GSH, the oxidized glutathione levels (GSSG) were also analyzed (Fig. 3b), showing no differences regarding control. As it is expected by the results of GSH and GSSG levels, the ratio GSH/GSSG changes due to HNE treatment, mainly depends on GSH contribution

(Fig. 3c). These results shown that the depletion of intracellular GSH can be associated with the formation of HNE adduct as has been previously shown in erythrocytes [27].

HNE Induces Apoptotic Cell Death in Neonatal Rat Cardiomyocytes

In order to discriminate whether HNE induced cell death by apoptosis or necrosis in NRC cultures, we have performed the following set of experiments: (1) analysis of hypodiploid peak by flow cytometry; (2) measurement of active caspase-3; (3) determination of the ratio ADP/ATP; and (4) LDH release assay.

Compared with the classic method of DNA ladder formation by gel electrophoresis for the determination of apoptosis, DNA content analysis by flow cytometry allows more accurate and quantitative measurements of apoptotic cells. This method is based on the presence of a hypodiploid peak, indicative of degraded DNA, manifested as a “sub-G1” peak on histograms (see Fig. 4a). Considering that nuclear fragmentation is a late apoptotic event [28], the cell cycle profile of neonatal rat cardiomyocytes was analyzed by flow cytometry after treatment with HNE during 3 h. We found that 5 and 10 μM HNE induced DNA breakdown (Fig. 4a). The analysis of hypodiploid peak

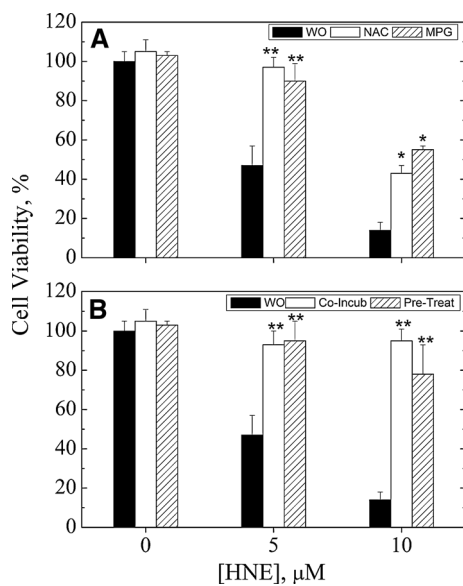


Fig. 2 Protection by NAC, MPG, and Trolox against HNE-induced cell death in cultured NRC: After 4th DIV, cells plated at 1×10^6 cells into 35-mm-diameter dishes were transferred to a serum-free medium, and 12 h later, the cells were exposed to 1 mM of NAC or MPG for 3 h (open and hatched histograms, respectively). Next, the medium containing NAC or MPG was replaced by fresh Locke K5 medium, and the cells were treated with 5–10 μM HNE or DMSO for 3 h (a). b Shows the effect of Trolox 200 μM . The incubation with this compound took place during treatment with HNE (co-incubation) or 1 h prior to HNE treatment (pretreatment) (open and hatched histograms, respectively). Viability was assessed by MTT reduction in all cases. All the results are expressed as the mean \pm SD for eight separate experiments * $p < 0.02$ and ** $p < 0.01$ (compared with vehicle, 5 μM HNE and 10 μM HNE, respectively)

area showed that HNE induces an increase in the peak area corresponding to “sub-G1” DNA, the extent of the increment being 3.7 and 4.3 times for 5 and 10 μM HNE, respectively, compared with control. The percentage of DNA hypodiploid were 44 and 51 %, respectively, while in the control sample, it was found to be 12 % (Fig. 4a). As expected, the DNA fragmentation that takes place after 3-h treatments with 5 and 10 μM HNE is prevented when the cardiomyocytes are pretreated for 3 h with NAC 1 mM (data not shown).

DNase activation (and therefore DNA fragmentation), in some cases, depends on caspase activity. We decided to assay the caspase-3 activity, which in addition is widely considered a good marker of apoptosis. For this purpose, caspase-3 activity was measured in vivo, after 1 h of treatment, because the activation of caspases is an early event in apoptosis onset [29]. The results, represented as positive cell versus total cell number in percentage, (Fig. 4b), show a significant increase in caspase-3 activity in cells treated with HNE compared with control cardiomyocytes, which supports the hypothesis of an apoptotic cell death as consequence of HNE treatment.

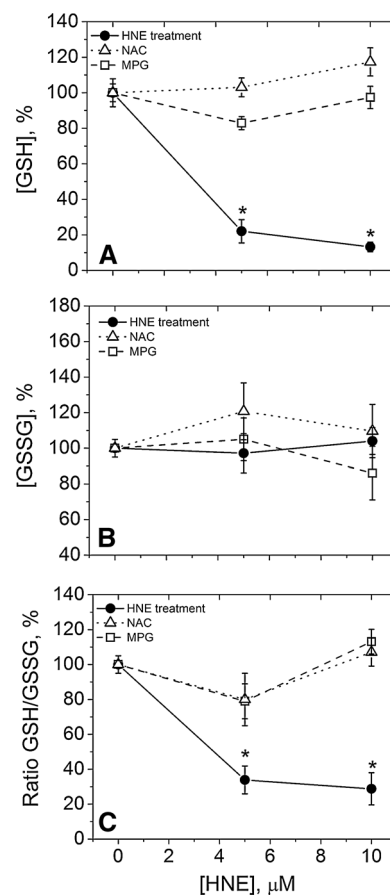


Fig. 3 Effect of exposure to different concentrations of HNE on the cellular glutathione level. Prevention of glutathione depletion by thiol compounds NAC and MPG: After 4th DIV, cells plated at 1×10^6 cells into 35-mm-diameter dishes were transferred to a serum-free medium, and 12 h later, they were incubated during 3 h with different HNE concentrations in Locke K5 medium (full circles). The treatment with 1 mM NAC or MPG was carried out for 3 h prior to HNE treatment. a GSH level in % of control. b GSSG level in percentage of control. c Ratio GSH/GSSG in percentage of control. The points (full circle: control; empty triangles: NAC; empty squares: MPG) are the experimental data, and the lines (solid: control; dash: NAC and dor: MPG) are merely to guide the eye. GSH content was calculated as indicated in “Materials and Methods”. All results are expressed as the mean \pm SD for four separate experiments * $p < 0.01$ (compared with control, vehicle treatment)

The cell energetic balance is another determining feature to distinguish between apoptosis and necrosis. The ratio ADP/ATP has been established as a useful tool for determining the type of cell death [30]. Therefore, after protein precipitation, the concentration of ATP and ADP was analyzed spectrophotometrically. The results obtained, represented in Fig. 4c as ADP/ATP ratio, showed values close to 1 in cells treated with HNE, whereas in control, the ratio ADP/ATP is approximately 0.2. Taking into account the data obtained in [30], the ADP/ATP ratios obtained in this paper are compatible with an apoptotic process, which supports our previous results of caspase-3 activation and

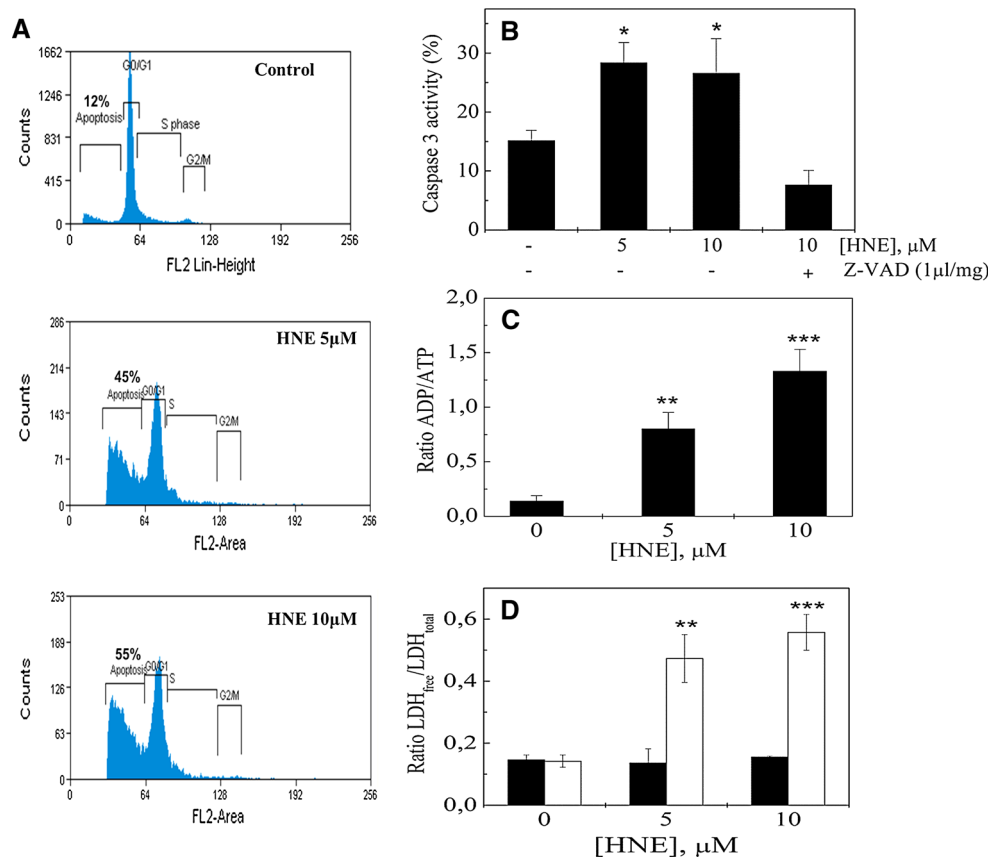


Fig. 4 Mechanism of HNE-induced cell death in cultured NRC: After 4° DIV, cells plated at 1×10^6 cells into 35-mm-diameter dishes were transferred to a serum-free medium, and 12 h later, they were treated with different HNE concentrations in Locke K5 medium. **a** HNE increases the hypodiploid DNA content in NRC: The cells were treated with 5 and 10 μM HNE following the standard protocol for 3 h; afterward, the nuclei extraction and cytometric analysis were done as is indicated in “Materials and Methods.” Values on the x -axis denote DNA content, and the values on y -axis denote cell counts. The hypodiploid peak is a marker of DNA fragmentation, a characteristic feature of apoptosis. **b** Measurement of active caspase-3: The cells were treated with HNE at the concentration indicated in the figure for 1 h. The treatment with 10 μM HNE in the presence of caspase inhibitor Z-VAD is employed as negative control. The protocol is

described in “Materials and Methods.” **c** Determination of ADP/ATP ratio: NRC were treated with 5 and 10 μM HNE for 3 h. ADP and ATP contents were determined spectrophotometrically after extraction with perchloric acid and neutralization with KOH as is described in “Materials and Methods.” **d** Measurement of LDH release: After incubating the cells with 5 and 10 μM HNE for 1.5 (*closed histograms*) and 3 h (*open histograms*), the LDH activity was spectrophotometrically evaluated, in the medium (LDH_{free}) as well as in the cell lysate (LDH_{cyt}), following the protocol described in “Materials and Methods.” Afterward, the ratio LDH_{free}/LDH_{total} was calculated. The data presented correspond to mean \pm SD ($N = 6$). Statistical analysis was carried out using one-way ANOVA followed by Tukey’s test. * $p \leq 0.05$; ** $p \leq 0.005$; *** $p \leq 0.0005$

DNA fragmentation. It is interesting to highlight the correlation between the ratio ADP/ATP and the estimation of the “sub-G1” fraction by PI staining and flow cytometry (Supplementary Material, Figure S2). The higher the percentage of hypodiploidy, the greater the ratio ADP/ATP, establishing a linear regression with $R = 0.99$. This result also fits with [30].

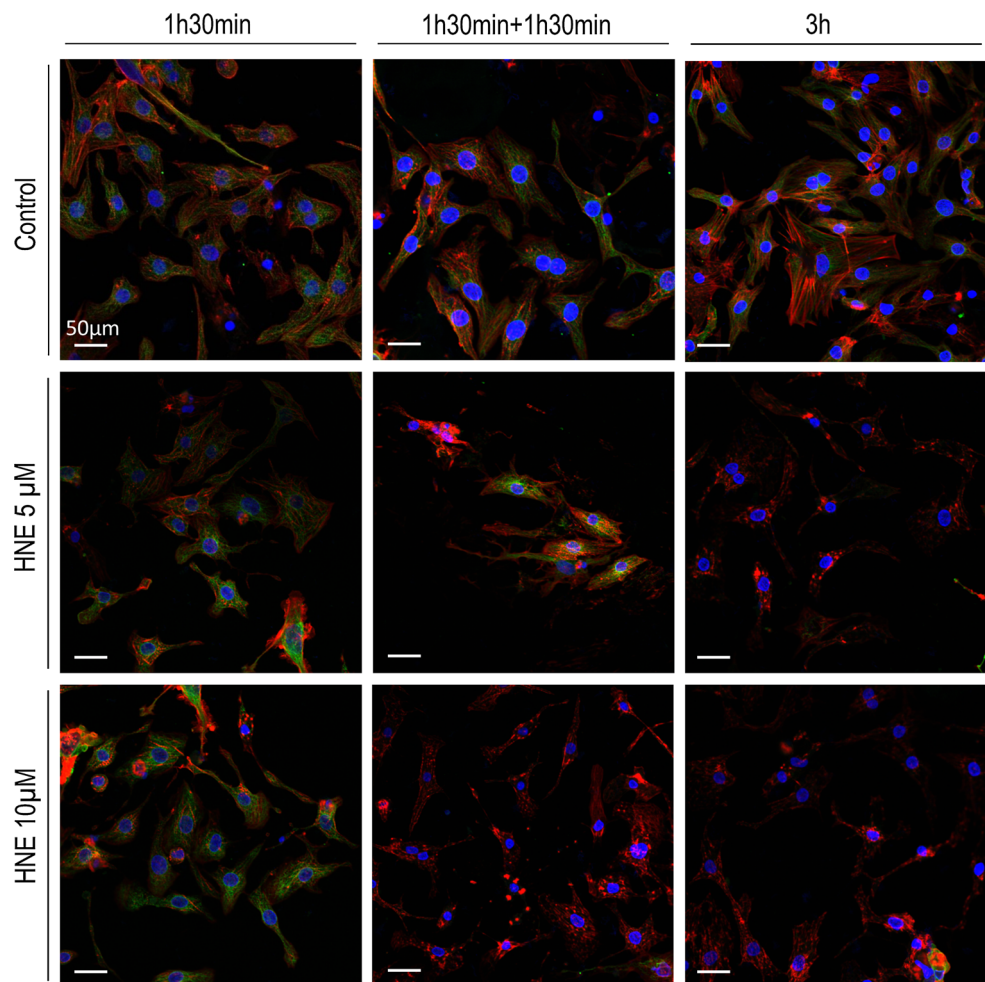
To definitely discard necrotic cell death after HNE treatments, we carried out LDH activity measurements. The analysis of LDH release performed after incubating the cells with HNE during 1.5 h shows no differences (Fig. 4d); however, a two- to threefold increase in LDH_{free}/LDH_{total} ratio is observed after 3-h treatment with 5 and 10 μM HNE, respectively (Fig. 4d). This feature is

compatible with the data of trypan blue viability, which assessed the cell viability through the permeability to this dye based on the disruption of cell membrane. These results could be explained as a feature observed in cultured cells undergoing apoptosis, in which the plasma membrane disruption occurs at the end of the process and it is called “secondary necrosis” [31].

Disruption of Cytoskeleton by HNE

Epifluorescence microscopic examination of HNE-treated cardiomyocytes incubated with anti- α -tubulin and rhodamine-phalloidin was carried out to detect microtubules and actin fibers, respectively. Figure 5 shows cytoskeleton

Fig. 5 Double fluorescence localization of actin and tubulin by rhodamine–phalloidin (red) and anti- α -tubulin (green), respectively, in neonatal rat cardiomyocytes control (upper row) and treated with 5 μ M (middle row) and 10 μ M (lower row) HNE: After 4^o DIV, cells plated in glass coverslip (21 \times 21 mm) were transferred to a serum-free medium, and 12 h later, they were treated for 1.5 or 3 h with different HNE concentrations in Locke K5 medium (first and third columns). In order to analyze the reversibility of the process, cells were treated for 1.5 h, and afterward, the medium was replaced by fresh serum-free medium, in which cells remained for 1.5 h (second column). Images shown are representative of different microscopic fields randomly taken from at least five experiments (Color figure online)



disruption after incubating the cells for 3 h with HNE. This is evident both as a loss of tubulin signal, consistent with a microtubules depolymerization process, and a loss of actin fibers that collapse generating big aggregates. This cytoskeleton disruption was not evident after 1.5 h (Fig. 5), a condition in which cell viability is not significantly different from control. The disruption of cytoskeleton by HNE has been previously reported after an acute treatment with doses higher than those employed for this work [32].

According to the fact that cell viability continues decreasing significantly when the media containing HNE are replaced by fresh media without the drug (data not shown), we decided to perform the study of the cytoskeleton disruption under a new condition. After incubating the cells with HNE for 1.5 h, the medium is replaced by fresh serum-free medium (without HNE), maintaining the cells in this new condition for an additional 1.5 h. The images of the second column in Fig. 5 show the same features described at 3 h, which means that the mechanism responsible for carrying out the cytoskeleton disorganization has been triggered during the first 1.5 h of treatment; therefore, the

elimination of HNE from the medium does not prevent the progression of cell damage.

Cytosolic Ca^{2+} Increase After HNE Treatment

$[\text{Ca}^{2+}]_i$ was measured using cardiomyocytes preloaded with the Ca^{2+} -fluorescent sensitive dye, fura-2 as described in “Materials and Methods.” Fig. 6b, where the Ca^{2+} level is represented as ratio 340/380 nm, shows an increase in calcium level after 15 min of treatment with HNE. This was not observed in control cells, where the Ca^{2+} level remained unaltered. Images in Fig. 6a illustrated these results, corresponding to control (upper image) and 10 μ M HNE after 15 min (bottom image). These results indicate that HNE-mediated elevation of cytoplasmic Ca^{2+} could be triggering apoptosis in neonatal rat cardiomyocytes.

In our cell model, the clusters of cardiomyocytes exhibit spontaneous and synchronous contractions, demonstrating the presence of mechanical and electrical continuities between cells via intercalated disks. The control cells (cardiomyocytes treated with DMSO) presented large

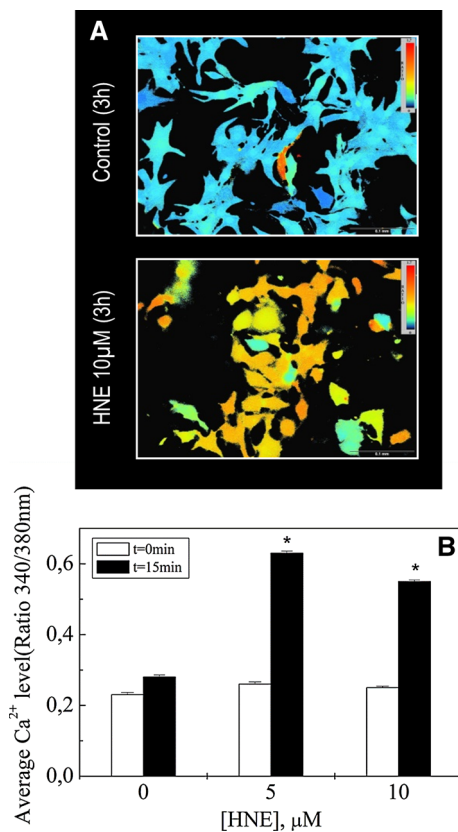


Fig. 6 Analysis of the increase in steady state $[\text{Ca}^{2+}]_i$ after exposure to 5 and 10 μM HNE: After 3rd DIV, cells plated in glass coverslip (21 \times 21 mm) were transferred to a serum-free medium and loaded with 10 μM fura-2-AM for 45 min. Afterward, the medium is replaced by Locke K5 supplemented with HNE (final concentrations 5 and 10 μM) or DMSO 0.1 % (HNE vehicle). The ratio 340/380 nm was obtained from fluorescence images just after adding HNE or DMSO 0.1 % (HNE vehicle) as indicated in “Materials and Methods.” **a** Shows the ratio images of fura-2-loaded NRC control and treated with 10 μM HNE for 3 h. The images are representative of different microscopic fields randomly taken from at least three experiments. **b** Statistical averages of the ratio (340/380 nm) values obtained at 0 and 15 min after the addition of HNE or DMSO in Locke K5. The results are expressed as the mean \pm SD for three separate experiments ($n \geq 25$ cells) * $p < 0.05$ (compared with control, vehicle treatment)

intracellular calcium transients associated with spontaneous beating at the beginning as well as after 15 min. Conversely, in cells treated with (5 and 10 μM) HNE, the spontaneous calcium transients are lost from the beginning of the treatment (data not shown).

Treatment of NRC with HNE Produces a Reduction of Mitochondrial Membrane Potential ($\Delta\Psi_m$) and ROS Generation

To determine $\Delta\Psi_m$, cells were loaded with TMRM 2 nM and Hoechst 33342 10 $\mu\text{g}/\text{mL}$ as described in “Materials and Methods.” Confocal microscopy images in Fig. 7b

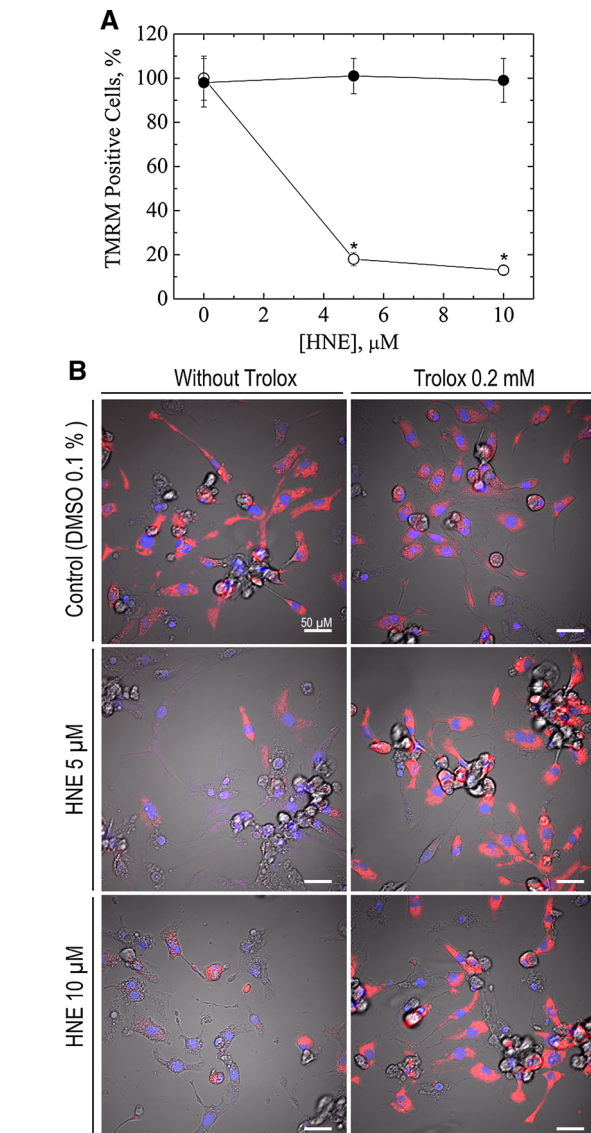


Fig. 7 HNE-induced decrease in mitochondrial membrane potential. Cells grown in glass coverslips were treated with HNE or DMSO for 1 h at 37 $^{\circ}\text{C}$ in medium Locke K5 (pH 7.4) in the absence or in the presence of Trolox 200 μM . After treatment, cells were incubated with TMRM 2 nM and Hoechst 33342 10 $\mu\text{g}/\text{mL}$ in PBS 1 \times for 30 min at 37 $^{\circ}\text{C}$. Intracellular fluorescence was visualized and recorded using an FV 1000 Olympus laser scanning confocal microscopy. Excitation and emission wavelengths were 550/590 nm for TMRM (red) and 405/440 nm for Hoechst 33342 (blue). **a**. Quantitative changes in mitochondrial membrane potential in cells treated with HNE in the absence (open circles) or in the presence of Trolox 200 μM (full circles). The results are expressed as the mean \pm SD for four separate experiments ($n \geq 50$ cells) * $p < 0.05$ (compared with control, vehicle treatment). **b**. The fluorescence images overlaid with the DIC-transmitted light. Images were acquired using a 40 \times objective and are representative of different microscopic fields randomly taken from at least four experiments (Color figure online)

(left column) show a loss of $\Delta\Psi_m$ in cardiomyocytes after HNE treatment, the fact that is supported by the TMRM fluorescence quantification, which decreased 80 and 90 %,

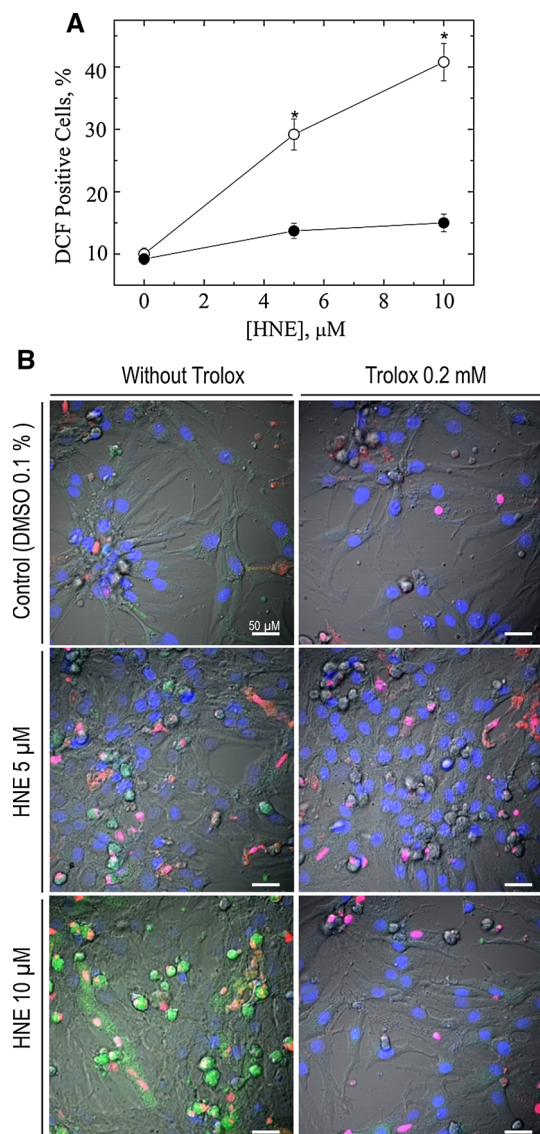


Fig. 8 ROS generation by HNE in NRC: Cells grown in glass coverslips were loaded with DCFH-DA 0.4 μM and Hoechst 33342 10 $\mu\text{g}/\text{mL}$ and treated with HNE or DMSO for 1 h at 37 $^{\circ}\text{C}$ in medium Locke K5 (pH 7.4) in the absence or in the presence of Trolox 200 μM . PI 3.75 μM was added to the medium just 5 min before analyzing. The DCF fluorescence was visualized and recorded using an FV 1000 Olympus laser scanning confocal microscopy. Excitation and emission wavelengths were 488/525 nm for DCF (green); 405/440 nm for Hoechst 33342 (blue); and 488/650 nm for PI (red). **a.** Quantitative changes in ROS level in cells treated with HNE in the absence (open circles) or presence (full circles) of Trolox 200 μM . The results are expressed as the mean \pm SD for four separate experiments ($n \geq 50$ cells) * $p < 0.05$ (different from control, vehicle treatment). **b.** The fluorescence images overlaid with the DIC-transmitted light. Images were acquired using a 40 \times objective and are representative of different microscopic fields randomly taken from at least three experiments (Color figure online)

regarding control, when cells are incubated for 1 h with 5 and 10 μM HNE, respectively (Fig. 7a—open symbols). Importantly, co-treatment with Trolox 200 μM exerts a

protective effect against the mitochondrial damage caused by HNE, with similar TMRM fluorescence levels to the control (Fig. 7b, right column and Panel A, full symbols).

We also evaluated ROS generation with confocal microscopy using the probe DCFH-DA on cardiomyocytes under control or treated conditions. The fluorescence images in Fig. 8b—left column—indicate a dramatic increase in DCF fluorescence, which is proportional to the level of intracellular ROS, as it is quantified in Fig. 8a. In this experimental set, HNE causes a concentration-dependent increase in intracellular ROS production. In fact, at treatments with concentrations of 5 and 10 μM HNE for 1 h, intracellular ROS level increased to approximately three- and fourfolds, respectively, compared with untreated cells (Fig. 8a—open symbols). As described before for $\Delta\Psi\text{m}$, HNE-induced ROS generation was prevented when cells were treated with HNE in the presence of 200 μM Trolox (Fig. 8b, right column and Panel A, full symbols), as expected for a compound with both antioxidant and free radical scavenger activities.

Discussion

4-Hydroxy-2-nonenal is a LP product generated from the breakdown of polyunsaturated fatty acids as a consequence of oxidant-mediated damage. HNE concentrations are elevated under pathological conditions such as cardiovascular diseases [10, 17]. Our results demonstrate that HNE can markedly induce cell death in neonatal rat cardiomyocytes at small concentrations (5–10 μM). These concentrations may be present in cells under the oxidative stress conditions that underlie several cardiovascular diseases such as MI, HF, and I/R. Recently, it has been shown that HNE at low doses (5 μM) can protect cardiac myocytes against cytotoxic concentrations of HNE (≥ 20 μM) via Nrf-2-dependent pathway [33]. The lack of cell death at 5 and 10 μM HNE reported in this paper does not agree with our results. It could be explained by the choice of the experimental conditions used to carry on the treatment with HNE, because it has previously been shown in different cell types that the cells became less sensitive to HNE treatment only if the treatment with HNE is performed in the presence of serum [34].

According to our results, the cell death induced by HNE takes place by an apoptotic process, evidenced by several apoptotic features such as DNA fragmentation and a decrease in the ratio ADP/ATP, which is compatible with the values established in [30] for apoptosis. Nevertheless, the most reliable marker of an apoptotic process is the activation of caspase-3 after 1 h of treatment with HNE. Additionally, the HNE-induced LDH release after 3 h of treatment, but not after a shorter incubation (1.5 h)

confirmed the maintenance of the cell membrane integrity until the end of the apoptotic process. Since loss of membrane integrity is a characteristic feature of necrosis, LDH release after 3-h treatment could fit with a secondary necrosis [31].

The precise sequential mechanism of 4-HNE-induced apoptosis is not clearly understood. Previous work showed the implications of Ca^{2+} overload and ROS on apoptosis induction and development by HNE in adult rat cardiomyocytes [18]. In the onset of apoptosis, Ca^{2+} can also trigger mitochondrial alterations [35]. Our experiments with fura-2 aimed to determine cytosolic Ca^{2+} level, showing that treatment with 5 and 10 μM HNE increases significantly the Ca^{2+} cytosolic level after 15 min of treatment. This fact could be tightly related to a previous work from our group, in which we showed that low HNE concentrations ($<20 \mu\text{M}$) disrupt calcium dynamic in SR vesicles, through a leakage of Ca^{2+} . The covalent modification of two luminal proteins implicated in the regulation of the ryanodine receptor (RyR) by HNE seems to be indirectly responsible for Ca^{2+} leak through RyR in SR vesicles [5]. In addition to Ca^{2+} overload, we observed a ROS burst and loss of mitochondrial membrane potential after 1 h in the presence of 5 and 10 μM HNE. Taking into account the critical role of mitochondria in mediating the cellular response to oxidants formed during acute and chronic cardiac dysfunction, we propose the alterations of mitochondrial function evidenced as critical events in the downstream development of cell death. Our findings agree with [36], in which an increase in oxygen consumption and a mitochondrial dysfunction were observed after exposure of cardiac myocytes to pathologically relevant concentrations of HNE. The time-course of the events observed point to a Ca^{2+} increase being responsible for triggering mitochondrial alterations and therefore cell death. Despite the fact that the exact apoptotic pathway is not established yet, our results fit with the intrinsic pathway more than the extrinsic one, although more work needs be carried out to establish the exact mechanisms. Another characteristic feature for the end stage of apoptosis is the depolymerization of cytoskeleton fibers, such as microtubules and actin microfilaments, reported in this work, which seem to be a direct consequence of caspase activity, due to the time-course of this event and the irreversibility of the process. Also, the ROS produced as consequence of HNE treatment could be responsible for triggering the oxidation of membrane lipids in a positive feedback loop [18]. Among other LP products, the lipid hydroperoxides are especially relevant, because they have proven even more toxic than HNE itself [37].

Due to the high reactivity of HNE for thiol groups [2], the GSH pool is depleted around 80 % after 3 h, the behavior being similar for 5 and 10 μM HNE, whereas no

changes in GSSG level are reported at these conditions. This fact can be due to the formation of GSH-HNE adducts, instead of GSH oxidation by HNE action. Taking into account the affinity of HNE for thiol residues, the thiol compounds NAC and MPG were tested to prevent the GSH depletion and cytotoxicity induced by HNE. The results showed that both compounds are able to prevent 100 % of GSH depletion. However, cell viability is avoided less effectively, which could mean that the implication of GSH depletion in the mechanism of cell death is not unique. Probably, apart from GSH depletion, other kinds of alterations, such as the Ca^{2+} overload or mitochondrial damage discussed above, have a co-operative influence in the mechanisms of cell death. This idea is supported by the fact that the antioxidant Trolox, whose scavenger activity is well known [38], exerts a higher degree of prevention of cell death induced by HNE. The role of GSH depletion in toxicity induced by HNE is explained by the fact that GSH is a central element in the cellular antioxidant defense and its loss renders cells more prone to oxidative stress. The GSH depletion seems to be through a covalent interaction between HNE and GSH to form the conjugate HNE-GS, since GSH depletion is not accompanied by an increase in GSSG. Besides, a relationship could be established between the loss of ATP and formation of HNE-GS conjugation, because HNE-GS conjugation is removed by a transporter of multidrug-resistance-associated proteins (MDRs), whose function is dependent on ATP hydrolysis [39]. Therefore, the enhancement of GSH depletion potentially results in an increase in ATP consumption. The loss of GSH pool following 3-h treatment is concomitant with the LDH release. Based on these features, the secondary necrosis described after 3 h in the presence of HNE could be explained according to the relationship between the fragility of sarcolemma and the depletion of GSH described in [40].

In conclusion, in this paper, we showed that pathophysiological doses of HNE cause cell death in neonatal rat cardiomyocytes, the LD_{50} being 4.4 μM at 3 h. The toxic effect of HNE is dose dependent, as well as time dependent, peaking at 3 h. It is the relevant increase in Ca^{2+} cytosolic level at the beginning of the treatment (15 min), which is accompanied by the loss of Ca^{2+} transients responsible for cell contraction. Apoptosis is the mechanism responsible for cell death in neonatal rat cardiomyocytes after treatment with HNE. Mitochondrial alterations (bursts of ROS and loss of $\Delta\Psi_m$) appear after 1 h of treatment with HNE, which could increase the cell damage induced by HNE, initiating the signal pathway responsible for caspase-3 activation. As a consequence of caspase-3 activity, DNA fragmentation occurs at the end of the cell death process. The decrease in ATP level, demonstrated after 3 h, is in agreement with an apoptotic process, which

supports the previous conclusion. The loss of membrane integrity described after 3-h treatment, but not after 1 h 30 min is a consequence of a secondary necrosis. It is related to the cytoskeleton alterations and the loss of GSH pool, which enhance the fragility of the sarcolemma. Of particular significance is that pretreatment with several antioxidant compounds prevents the toxic effect of HNE in neonatal rat cardiomyocyte, thus opening new avenues for drug discovery.

Acknowledgments We are grateful to Dr. Iffath Ghouri and Dr. Jose María Carvajal-González for their helpful discussion and critical reading of the manuscript. Technical and human support provided by Facility of Bioscience Applied Techniques (STAB) of Servicios de Apoyo a la Investigación (SAIUEx) (financed by Universidad de Extremadura, Junta de Extremadura, Ministerio de Ciencia e Innovación, Fondo Europeo de Desarrollo Regional-FEDER). This work was supported by a Grant from the Junta de Extremadura, Spain (PRI06A132 to F. Henao; GRU09056 and GRU10046 to Grupo de Investigación en Enfermedades Neurodegenerativas). M.P.H.-V. had been the recipient of predoctoral fellowships from the Junta de Extremadura (Spain). All Spanish funding is co-sponsored by the European Union FEDER (Fondo Europeo de Desarrollo Regional) program.

Conflict of interest The authors declare that they have not conflict of interest.

References

- Grassi, D., Desideri, G., Tiberti, S., & Ferri, C. (2009). Oxidative stress, endothelial dysfunction and prevention of cardiovascular diseases. *AgroFOOD Industry Li-tech*, *20*, 76–79.
- Esterbauer, H., Schaur, R. J., & Zollner, H. (1991). Chemistry and biochemistry of 4-hydroxynonenal, malonaldehyde and related aldehydes. *Free Radical Biology & Medicine*, *11*, 81–128.
- Uchida, K. (2003). 4-Hydroxy-2-nonenal: A product and mediator of oxidative stress. *Progress in Lipid Research*, *42*, 318–343.
- Anderson, E. J., Katunga, L. A., & Willis, M. S. (2011). Mitochondria as a source and target of lipid peroxidation products in healthy and diseased heart. *Clinical and Experimental Pharmacology and Physiology*, *39*, 179–193.
- Hortigón-Vinagre, M. P., Chardonnet, S., Montigny, C., Gutiérrez-Martín, Y., Champeil, P., & Henao, F. (2011). Inhibition by 4-hydroxynonenal (HNE) of Ca²⁺ transport by SERCA1a: Low concentrations of HNE open protein-mediated leaks in the membrane. *Free Radical Biology & Medicine*, *50*, 1700–1713.
- Leonarduzzi, G., Chiarpotto, E., Biasi, F., & Poli, G. (2005). 4-Hydroxynonenal and cholesterol oxidation products in atherosclerosis. *Molecular Nutrition & Food Research*, *49*, 1044–1049.
- Yun, M. R., Im, D. S., Lee, S. J., Woo, J. W., Hong, K. W., Bae, S. S., et al. (2008). 4-hydroxynonenal contributes to macrophage foam cell formation through increased expression of class A scavenger receptor at the level of translation. *Free Radical Biology & Medicine*, *45*, 177–183.
- Mak, S., Lehotay, D. C., Yazdanpanah, M., Azevedo, E. R., Liu, P. P., & Newton, G. E. (2000). Unsaturated aldehydes including 4-OH-nonenal are elevated in patients with congestive heart failure. *Journal of Cardiac Failure*, *6*, 108–114.
- Kloner, R. A., Przyklenk, K., & Whittaker, P. (1989). Deleterious effects of oxygen radicals in ischemia/reperfusion. Resolved and unresolved issues. *Circulation*, *80*, 1115–1127.
- Palojoki, E., Saraste, A., Eriksson, A., Pulkki, K., Kallajoki, M., Voipio-Pulkki, L. M., et al. (2001). Cardiomyocyte apoptosis and ventricular remodeling after myocardial infarction in rats. *American Journal of Physiology Heart and Circulatory Physiology*, *280*, H2726–H2731.
- Chiong, M., Wang, Z. V., Pedrozo, Z., Cao, D. J., Troncoso, R., Ibacache, M., et al. (2011). Cardiomyocyte death: mechanisms and translational implications. *Cell Death and Disease*, *2*, e244.
- Elmore, S. (2007). Apoptosis: A review of programmed cell death. *Toxicologic Pathology*, *35*, 495–516.
- Abarikwu, S. O., Pant, A. B., & Farombi, E. O. (2012). 4-Hydroxynonenal induces mitochondrial-mediated apoptosis and oxidative stress in SH-SY5Y human neuronal cells. *Basic & Clinical Pharmacology & Toxicology*, *110*, 441–448.
- Cheng, J. Z., Sharma, R., Yang, Y., Singhal, S. S., Sharma, A., Saini, M. K., et al. (2001). Accelerated metabolism and exclusion of 4-hydroxynonenal through induction of RLIP76 and hGST5.8 is an early adaptive response of cells to heat and oxidative stress. *Journal of Biological Chemistry*, *276*, 41213–41223.
- Ji, B., Ito, K., & Horie, T. (2004). Multidrug resistance-associated protein 2 (MRP2) enhances 4-hydroxynonenal-induced toxicity in Madin-Darby canine kidney II cells. *Chemical Research in Toxicology*, *17*, 158–164.
- Nicotera, P., & Orrenius, S. (1986). Role of thiols in protection against biological reactive intermediates. *Advances in Experimental Medicine and Biology*, *197*, 41–51.
- Dhalla, N. S., Temsah, R. M., & Netticadan, T. J. (2000). Role of oxidative stress in cardiovascular diseases. *Hypertension*, *18*, 655–673.
- Nakamura, K., Miura, D., Kusano, K. F., Fujimoto, Y., Sumita-Yoshikawa, W., Fuke, S., et al. (2009). 4-Hydroxy-2-nonenal induces calcium overload via the generation of reactive oxygen species in isolated rat cardiac myocytes. *Journal of Cardiac Failure*, *15*, 709–716.
- Soares, S. S., Henao, F., Aureliano, M., & Gutiérrez-Merino, C. (2008). Vanadate induces necrotic death in neonatal rat cardiomyocytes through mitochondrial membrane depolarization. *Chemical Research in Toxicology*, *21*, 607–618.
- Gutiérrez-Martín, Y., Martín-Romero, F. J., Henao, F., & Gutiérrez-Merino, C. (2005). Alteration of cytosolic free calcium homeostasis by SIN-1: High sensitivity of L-type Ca²⁺ channels to extracellular oxidative/nitrosative stress in cerebellar granule cells. *Journal of Neurochemistry*, *92*, 973–989.
- Morales-Hernández, A., Sánchez-Martín, F. J., Hortigón-Vinagre, M. P., Henao, F., & Merino, J. M. (2012). 2,3,7,8-Tetrachlorodibenzo-p-dioxin induces apoptosis by disruption of intracellular calcium homeostasis in human neural cell line SHSY5Y. *Apoptosis*, *17*, 1170–1181.
- Hallmann, A., Milczarek, R., Szkatuła, M., Woźniak, M., Spodnik, J. H., & Klimek, J. (2005). Mimicking of glutathione peroxidase deficiency by exposition of JAR cells to increased level of synthetic hydroperoxide. *Folia Morphol (Warsz)*, *64*, 304–308.
- Dominguez-Rodríguez, A., Abreu-Gonzalez, P., de la Rosa, A., Vargas, M., Ferrer, J., & García, M. (2005). Role of endogenous interleukin-10 production and lipid peroxidation in patients with acute myocardial infarction treated with primary percutaneous transluminal coronary angioplasty interleukin-10 and primary angioplasty. *International Journal of Cardiology*, *99*, 77–81.
- Mak, S., Lehotay, D. C., Yazdanpanah, M., Azevedo, E., Liu, P., & Newton, G. E. (2000). Unsaturated aldehydes including 4-OH-nonenal are elevated in patients with congestive heart failure. *Journal of Cardiac Failure*, *6*, 108–114.

25. Townsend, D. M., Tew, K. D., & Tapiero, H. (2003). The importance of glutathione in human disease. *Biomedicine & Pharmacotherapy*, *57*, 145–155.
26. Arakawa, M., & Ito, Y. (2007). *N*-acetylcysteine and neurodegenerative diseases: Basic and clinical pharmacology. *Cerebellum*, *19*, 1–7.
27. Biswas, D., Sen, G., & Biswas, T. (2010). Reduced cellular redox status induced 4-hydroxynonenal-mediated caspase 3 activation leading to erythrocyte death during chronic arsenic exposure in rats. *Toxicology and Applied Pharmacology*, *244*, 315–327.
28. Collins, J. A., Schandi, C. A., Young, K. K., Vesely, J., & Willingham, M. C. (1997). Major DNA fragmentation is a late event in apoptosis. *Journal of Histochemistry and Cytochemistry*, *47*, 923–934.
29. Telford, W. G., Komoriya, A., & Packard, B. Z. (2002). Detection of localized caspase activity in early apoptotic cells by laser scanning cytometry. *Cytometry*, *47*, 81–88.
30. Bradbury, D. A., Simmons, T. D., Slater, K. J., & Crouch, S. P. (2000). Measurement of the ADP:ATP ratio in human leukemic cell lines can be used as an indicator of cell viability, necrosis and apoptosis. *Journal of Immunological Methods*, *240*, 79–92.
31. Vanden Berghe, T., Vanlangenakker, N., Parthoens, E., Deckers, W., Devos, M., Festjens, N., et al. (2010). Necroptosis, necrosis and secondary necrosis converge on similar cellular disintegration features. *Cell Death and Differentiation*, *17*, 922–930.
32. VanWinkle, W. B., Snuggs, M., Miller, J. C., & Buja, L. M. (1994). Cytoskeletal alterations in cultured cardiomyocytes following exposure to the lipid peroxidation product, 4-hydroxynonenal. *Cell Motil Cytoskeleton*, *28*, 119–134.
33. Zhang, Y., Sano, M., Shinmura, K., Tamaki, K., Katsumata, Y., Matsuhashi, T., et al. (2010). 4-Hydroxy-2-nonenal protects against cardiac ischemia-reperfusion injury via the Nrf2-dependent pathway. *Journal of Molecular and Cellular Cardiology*, *49*, 576–586.
34. Zarkovic, N., Schaur, R. J., Puhl, H., Jurin, M., & Esterbauer, H. (1994). Mutual dependence of growth modifying effects of 4-hydroxynonenal and fetal calf serum in vitro. *Free Radical Biology & Medicine*, *16*, 877–884.
35. Rong, Y., & Distelhorst, C. W. (2008). Bcl-2 protein family members: Versatile regulators of calcium signaling in cell survival and apoptosis. *Annual Review of Physiology*, *70*, 73–91.
36. Hill, B. G., Dranka, B. P., Zou, L., Chatham, J. C., & Darley-Usmar, V. M. (2009). Importance of the bioenergetic reserve capacity in response to cardiomyocyte stress induced by 4-hydroxynonenal. *Biochemical Journal*, *424*, 99–107.
37. Iliou, J. P., Thollon, C., Villeneuve, N., Robin, F., Cambarrat, C., Jacquemin, C., et al. (1995). Monohydroperoxidized fatty acids but not 4-hydroxynonenal induced acute cardiac cell damage. *Free Radical Biology & Medicine*, *19*, 773–783.
38. Hamad, I., Arda, N., Pekmez, M., Karaer, S., & Temizkan, G. (2010). Intracellular scavenging activity of Trolox (6-hydroxy-2,5,7,8-tetramethylchroman-2-carboxylic acid) in the fission yeast, *Schizosaccharomyces pombe*. *Journal of Natural Science, Biology, and Medicine*, *1*, 16–21.
39. Higgins, C. F. (1995). The ABC of channel regulation. *Cell*, *82*, 693–696.
40. Obermayr, R. P., Schlüter, K. D., Schäfer, M., Spieckermann, P. G., & Piper, H. M. (1999). Protection of reoxygenated cardiomyocytes against sarcolemmal fragility: the role of glutathione. *Pflügers Archiv. European Journal of Physiology*, *438*, 365–370.